Force networks in dense granular media

Farhang Radjai, D.E. Wolf, Stéphane Roux, Michel Jean, Jean Jacques
Moreau

HAL Id: hal-01824792
https://hal.science/hal-01824792

Submitted on 27 Jun 2018

Force networks in dense granular media

F. Radjai & D. E Wolf
Theoretische Physik, Gerhard-Mercator Universität, Duisburg, Germany

S. Roux
LPMMH, École Supérieure de Physique et Chimie Industrielles, Paris, France

M. Jean
IMT-LMA, Technopole de Château-Gombert, Marseille, France

J. J. Moreau
LMGC, Université des Sciences et Techniques, Montpellier, France

ABSTRACT: Using Contact Dynamics simulations of quasistatically driven assemblies of rigid particles we show that the contact network at every stage of deformation is composed of two complementary subnetworks: a "strong" percolating subnetwork of the contacts carrying a force larger than the mean force, and a "weak" subnetwork of the contacts carrying a force lower than the mean force. In the strong subnetwork, all contacts are nonsliding and forces have a decreasing exponential distribution. Almost the whole dissipation takes place inside the weak subnetwork, where the number of normal forces decays as a power-law. The strong subnetwork supports all the deviatoric load, whereas the weak subnetwork contributes only to the mean pressure. The orientation of the induced anisotropy (major principal axis of the fabric tensor) in the strong subnetwork is the same as that of the stress tensor, but the orientation of the induced anisotropy in the weak subnetwork is orthogonal.

1 INTRODUCTION

The internal mechanical state of a random packing of noncohesive particles is doubly *heterogeneous*:

1. Contact forces vary by several orders of magnitude on a scale far larger than the particle size (Dantu 1957, Liu et al. 1995);

2. Frictional dissipation (due to sliding) in quasistatic deformation occurs only at a small fraction of contacts.

Micromechanical modeling of granular materials involves a quantitative characterization of both statistical distributions and spatio-temporal correlations of internal variables on the scale of these heterogeneities. In this paper, on the basis of numerical results from simulations of a few thousands of particles in two dimensions, we show that the organization of these variables has a basic *bimodal* character, which is also reflected in the structure of the stress tensor. We will first briefly introduce the simulation method. Then, we will focus successively on force distributions, stress tensor, induced anisotropy, and dissipation.

2 SIMULATION METHOD

A numerical simulation of a densely-packed system has to tackle a *multicontact* problem. Every collision in such a medium is a multiple collision that cannot be reduced to a set of independent binary collisions since impulsions propagate through the contact network and may even leave the system. In the same way, the frictional resistance to shear is a collective phenomenon involving the mobilization of friction at kinematically correlated contacts. Another basic problem is that the contact laws are strongly *nonlinear*. In the approximation of perfectly rigid particles, the normal force at a contact is not given locally as a function of the relative displacement of two particles, but rather as a result of the global geometrical configuration of the whole system and the boundary conditions. Furthermore, the basic Coulomb's law of friction is *nonsmooth* in the sense that the relation between the relative tangential velocity and the friction force cannot be represented as a mathematical function. The Contact Dynamics (CD) method, which was used for the investigations reported in this paper, takes these features into account on a mathematical basis derived from Convex Analysis (Moreau 1994, Jean 1995). On one hand, the conditions of *perfect rigidity* and *exact Coulombian friction* are implemented with no resort to any regularization. On the other hand, all kinematic constraints are *simultaneously* taken into account, together with the equations of dynamics, in order to determine contact forces and particle velocities in the system. The method is thus able to deal properly with the nonlocal character of the momentum transfers in the contact network.
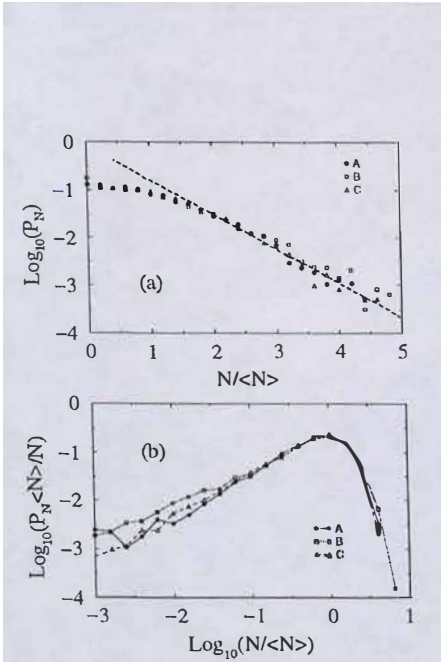
Figure 1. (a) Semilogarithmic, and (b) log-log plots of the probability distribution P_N of normal forces N.

3 FORCE DISTRIBUTIONS

Let us begin with the probability distribution P_N of normal forces N independently of contact orientations. Numerical results will be presented here for three samples of 4012, 4025, and 4098 particles, referred to as samples A, B, and C. Particles are contained in a rectangular frame composed of two horizontal and two vertical rigid walls. Sample A is biaxially compressed by allowing the inward motion of a horizontal wall and by applying a confining load on a vertical wall free to move horizontally. Sample B is in relaxation towards static equilibrium under a confining load applied to a free wall. Sample C is in static equilibrium under confining loads. The acceleration of gravity and the particle-wall coefficients of friction are set to zero. The interparticle coefficient of friction is 0.5 in samples A and C, and 0.2 in sample B. In all samples, the particle radii are uniformly distributed between 3.8 and 7.5 mm.

Figs. 1(a) and 1(b) display the plot of P_N on semilog and log-log scales in the three samples. In all cases, independently of the confining load, the normal forces lower than the mean normal force $\langle N \rangle$ have a power-law distribution, whereas the data for forces larger than $\langle N \rangle$ are well fitted by an exponential decay:

$$P_N \propto \begin{cases} \left(\dfrac{N}{\langle N \rangle} \right)^{-\alpha} & N < \langle N \rangle, \\ e^{\,\beta(1 - N/\langle N \rangle)} & N > \langle N \rangle. \end{cases} \quad (1)$$

Within the statistical precision, the values of exponents α and β depend only weakly on the mechanical parameters and the preparation conditions of each sample. In static equilibrium or in quasistatic deformation, the value of α is very close to

zero. However, it seems that α increases with the degree of dynamics inside the system and decreases with the coordination number. Let us also remark that, since the mean value $\langle N \rangle$ separates the two parts of the distribution, α and β should be related together by the equation $\beta^2 = (1-\alpha)(2-\alpha)$, which is approximately satisfied in our simulations.

As far as the distribution P_T of the absolute values of friction forces T is concerned, we *always* find a power law decay for forces lower than the mean friction force $\langle T \rangle$ and a decreasing exponential function for friction forces higher than $\langle T \rangle$, as shown in Figs. 2(a) and 2(b). This distinction between the forces lower than the mean, to which we will refer as "weak" forces, and those larger than the mean, referred to as "strong" forces in the following, has a deep meaning, as we shall see below. Let us only mention here that the exponential distribution of strong forces does not seem to be a finite-size effect. In other words, a simple normalization of the forces with respect to the mean force allows the data to collapse almost on the same curve (Radjai et al. 1996).

The exponential distribution of strong normal forces, has been observed in experiments (Liu et al. 1995, Miller et al. 1996). Weak normal forces and friction forces at individual contacts are technically difficult to measure, and their distributions have not yet been observed experimentally. The power-law decay or the uniform distribution of weak forces, comprising nearly 60% of contacts, indicates that the weak forces are generated through a self-similar branching process from strong forces. In contrast, the strong forces are conditionned by the level of the deviatoric load, which sets in effect a characteristic force different from the mean force. This point will become more clear by the study of the stress tensor.
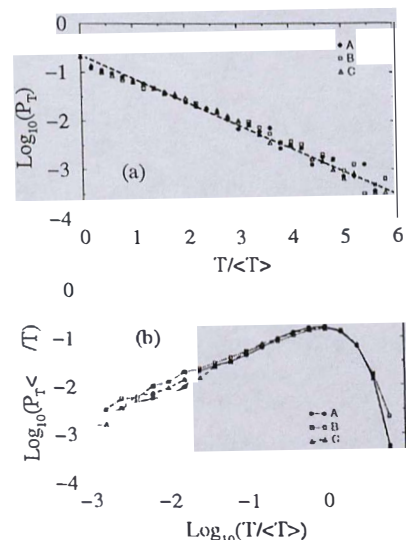

Figure 2. (a) Semilogarithmic, and (b log-log plots of the probability distribution P_T of friction forces T.
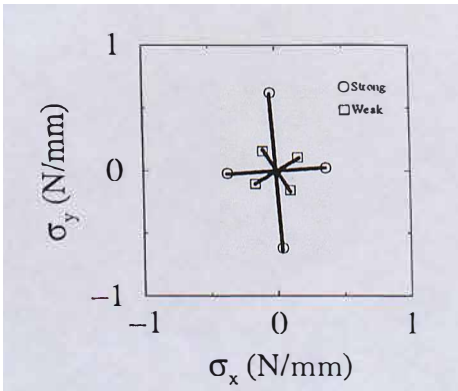
2

Figure 3. Contributions of weak and strong contacts to the stress tensor in sample A at shear peak.

4 STRESS TENSOR

The stress tensor is the relevant variable in transition to the continuous limit and, in contrast to P_N and P_T, involves both the contact forces and the contact orientations according to the following classical formula (Christoffersen et al. 1981): $\sigma_{ij} = \frac{1}{V(\Omega)} \sum_{c \in \Omega} f_i^c \, d_j^c$, where Ω is the region inside the sample for which the stress tensor is calculated with a volume equal to V, f_i^c is the i-component of the force at the contact c, and d_j^c is the j-component of the intercenter vector $\boldsymbol{d}^c$. This equation allows to separate the contributions of weak and strong forces to the global stress tensor. The weak tensor σ^w and the strong tensor σ^s are given by the above equation when the summation is restricted to only weak contacts and only strong contacts, respectively.

Among our samples, only sample A, due to its uniform stress field, provides enough statistics for the study of the stress tensor. Figure 3 shows the orientations and the eigenvalues of σ^w and σ^s in sample A at shear peak, i.e. at the maximal value of $q = \frac{\sigma_1 - \sigma_2}{\sigma_1 + \sigma_2}$, $(q = 0.18)$, where σ_1 and σ_2 are the principal values of the total stress tensor. We see that σ^w is almost spherical and contributes no more than 3% to the deviatoric part of the total stress tensor $\sigma = \sigma^w + \sigma^s$, whereas σ^s represents almost the whole deviatoric load, and its major principal axis has the same orientation as that of the imposed deformation.

The isotropic nature of the weak stress tensor indicates that the weak contacts feel the influence of the deviatoric load only as an average over all directions. The strong contacts directly support the deviatoric load, whose signature appears as a characterstic force in the exponential decay of strong forces.

5 INDUCED ANISOTROPY

We now consider the distribution P_θ of contact orientations. The anisotropic nature of P_θ has been extensively studied in the past (Biarez & Wiendick 1963, Satake 1978, Cambou & Sidoroff 1985, Rothenburg & Bathurst 1989). Here, we define two separate distributions P_θ^w and P_θ^s for weak and strong contacts, respectively. The polar diagrams of these distributions are shown in Figure 4 for sample A at shear peak. We see that both distributions are anisotropic, although to a lesser extent in the weak subnetwork than in the strong one. The interesting behavior observed here is that the principal direction of P_θ^s coincides with that of the stress tensor, whereas the principal direction of P_θ^w is *orthogonal*! This again confirms the bimodal nature of the force network, and clearly shows the *complementarity* between the two subnetworks: The strong chains need "lateral" weak forces in order to be stabe.
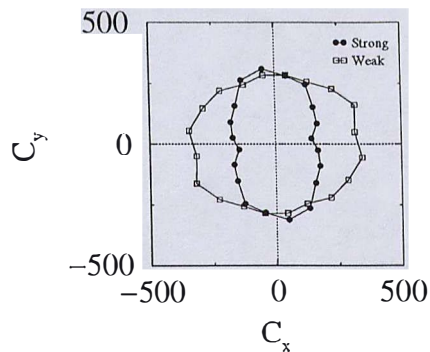

Figure 4. Polar diagram of the distribution of contact orientations in weak and strong subnetworks.

6 DISSIPATION

In a quasistatically driven system, the particle rotations are generally *frustrated*, with patterns that have been partially studied in the case of regular packings (Radjai & Roux 1995, Radjai et al. 1996). The possibility of particles to roll over one another provides a very low-dissipative local mechanism of deformation, so that if each particle could roll over its neighbors, then a dense granular system would essentially behave like a liquid. The question we raise here is how the positions of *sliding* contacts on the contact network are correlated with the contact forces?

The distinction between weak and strong subnetworks again provides a simple key to the problem. In Figure 5, we have shown the two subnetworks with different gray levels and the positions of the sliding contacts. Almost 8% of contacts are sliding, and a rapid inspection shows that almost all of them are on the weak subnetwork. In other words, all strong contacts are nonsliding and all the dissipation takes within the weak subnetwork. This remarkably simple behavior of the sliding contacts with respect to the force subnetworks shows the *dynamic* nature of the bimodal

3

distribution of forces. The strong subnetwork is *completely* unstable since all its contacts are nonsliding. As a result, it tends to buckle under the action of the external deviatoric load, giving rise to an orthogonal anisotropy and sliding contacts in the weak subnetwork.
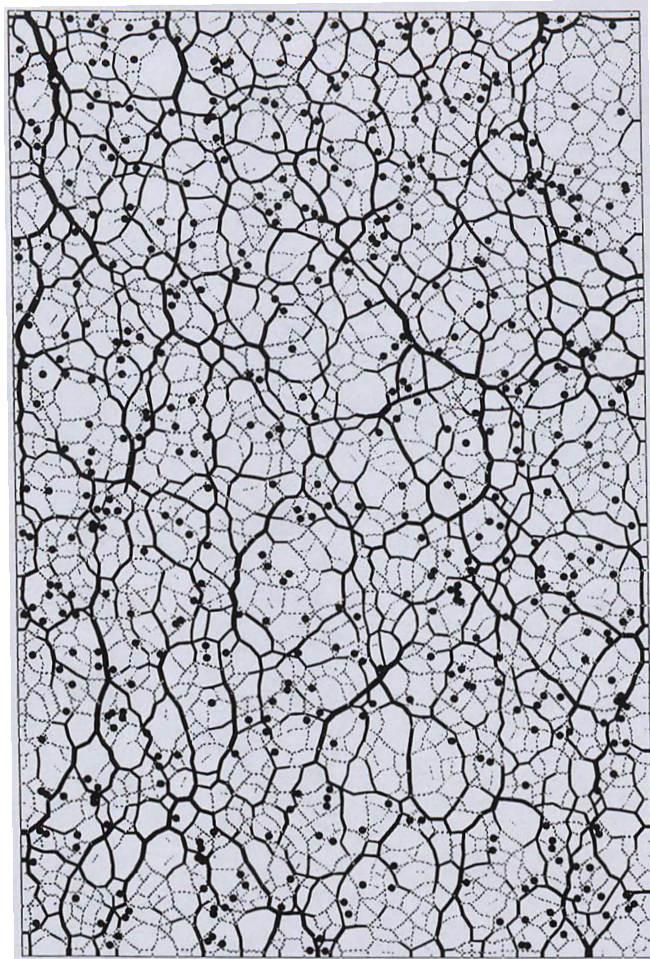

Figure 5. Network of normal forces in sample A. Forces are encoded as the widths of intercenter segments. Weak and strong subnetworks are shown with two different gray levels. The filled circles show the positions of sliding contacts.

7 CONCLUSION

The observations briefly presented above provide a simple picture of the internal state of a granular packing in quasistatic deformation, at least in two dimensions. The contact network is composed of two complementary subnetworks:

1. A "load-bearing" percolating subnetwork composed of strong contacts;

2. A "dissipative" subnetwork composed of weak contacts.

The strong subnetwork supports the whole deviatoric load applied on the system, although it contains only nonsliding (nondissipative) contacts. The whole dissipation takes place inside the weak subnetwork. This implies that the scale of heterogeneity of a granular system due to sliding and nonsliding states of contacts is the same as that of the strong subnetwork. From the point of view of the stress tensor, the weak subnetwork behaves like an intersticial liquid, whereas the strong subnetwork has a solid-like behavior since it takes over the whole deviatoric load and thus the stability of the system. From the point of view of the fabric tensor (or contact orientations), the strong subnetwork bears the *primary* anisotropy induced by shear, but it gives rise to a *secondary* orthogonal anisotropy inside the weak subnetwork.

This bimodal behavior of the force network opens new perspectives both for microscopic and macroscopic modeling of granular materials in quasistatic deformation. Let us, however, recall that the analysis presented here concerns a two-dimensional system. It is not obvious that it applies in the same manner to three-dimensional systems. Therefore, the investigation of three-dimensional systems, even though their simulation is more involved, is crucial to the further establishment of the results presented in this paper.

REFERENCES

Biarez J. & Wiendick K. 1963. C. R. Acad. Sci. **256**: 1217.

Cambou B. & Sidoroff F. 1985. J. Mech. Th. Appl. **4**(2): 223.

Christoffersen J., Mehrabadi M. M. & Nemat-Nasser S. 1981. J. Appl. Mech. **48**: 339.

Dantu P. 1957. In *Proceedings of the 4th International Conference on Soil Mechanics and Foundations Engineering*. London: Butterworths Scientific Publications.

Jean M. 1995. In A. P. S. Selvadurai & M. J. Boulon (eds.), *Mechanics of Geometrical Interfaces*. Amsterdam: Elsevier.

Liu C.-h., Nagel S. R., Schecter D. A., Coppersmith S. N., Majumdar S., Narayan O. & Witten T. A. 1995. Science **269**: 513.

Moreau J. J. 1994. Eur. J. Mech. A/Solids **13**, n° 4-suppl.: 93.

Miller B., O'Hern C. & Behringer R. P. 1996. Phys. Rev. Lett. **77**: 3110.

Radjai F., Jean M., Moreau J.J. & Roux S. 1996. Phys. Rev. Lett. **77**: 274.

Radjai F. & Roux S. 1995. Phys. Rev. E **51**: 6177.

Radjai F., Brendel L. & Roux S. 1996. Phys. Rev. E **54**: 861.

Rothenburg L. & Bathurst R. J 1989. Géotechnique **39**(4): 601.

Satake M. 1978. In *Theoretical and Applied Mechanics*: 257. Tokyo: Tokyo University Press.